ESAFORM 25 YEARS ON

Plasticity evolution of an aluminum-magnesium alloy under abrupt strain path changes

Junhe Lian[1] · Wenqi Liu[1] · Xabier Gastañares[1,2] · Rongfei Juan[1] · Joseba Mendiguren[2]

Abstract

During the forming and manufacturing of engineering materials, plasticity behavior could be evolving significantly due to complex deformation history. Therefore, this study aims to characterize the plasticity evolution of an aluminum-magnesium alloy under simple monotonic and non-monotonic loading with abrupt strain path changes. Instead of focusing only on one single stress state in the first-step loading for most of the studies in the literature, the current non-monotonic strain path testing program investigates three stress states – uniaxial, plane-strain, and biaxial tension – in the first-step loading and combines them with a second-step uniaxial loading along and orthogonal to the initial loading direction. This combination generates non-monotonic stress–strain data in a quite large and distributed spectrum in terms of the Schmitt parameter. It is found that the aluminum-magnesium alloy shows a unique phenomenon with a lower yield strength at reloading compared to monotonic cases coupled with a steady increase of stress overshooting the monotonic one at large strains. This increase of stress as well as the strain hardening rate lasts till the uniform strain and is therefore referred to as permanent hardening. The comprehensive non-monotonic behavior delivered by the new experimental program in this study could further assist the development of material models and an in-depth understanding of the underlying mechanisms.

Keywords Non-monotonic loading · Cross loading · Permanent hardening · Dynamic strain aging · Anisotropic hardening · AA5754

Introduction

Material forming, as one of the most important techniques to convert raw materials to final products, has a significant impact on almost all industrial engineering applications. For metallic materials, plastic deformation is heavily involved in any simple (e.g., rolling, forging) or much more complicated forming technologies (e.g., stamping, machining). One demanding and common vision in this field for both material and mechanical engineers is to understand and predict the plastic deformation behavior of metals during and after these forming processes. However, it is also a very challenging goal, as the forming processes typically impose many operation conditions, such as a large range of temperatures and strain rate in certain cases, and more commonly a complex local loading history in terms of stress states and loading directions, which could result in sophisticated microstructure and property evolution.

The investigation of plastic behavior evolution over loading history in the literature has been mainly focusing on two types of tests or phenomena: i) reverse or cyclic loading and ii) loading with a non-monotonic strain path. Cyclic loading has been investigated with a long history and the dominant loading mode is uniaxial tension–compression reverse/cyclic loading with particularly symmetric loads for both tension and compression sides. Other common concerned loading types are reverse or cyclic simple shear and torsion conditions. For the case with a non-monotonic strain path, the common investigation strategy is combining two individual monotonic or even linear strain paths to simplify the problem. By playing with two loading variables, stress state, and loading direction, two approaches have been established due to the concerned material mechanical properties, i) the

✉ Junhe Lian
 junhe.lian@aalto.fi

1 Advanced Manufacturing and Materials, Department of Mechanical Engineering, Aalto University, Puumiehenkuja 3, 02150 Espoo, Finland

2 Mechanical and Industrial Manufacturing Department, Mondragon University, Loramendi 4, 20500 Mondragon, Spain

forming limit (strain) sensitive approach and ii) the stress-sensitive approach.

The non-monotonic strain path influence on the forming limits of metallic materials has been studied since about a half-century ago with experimental work followed by theoretical modeling [1–6]. Typical tests involved in these results are either the classic Nakajima tests or Marciniak tests. Normally, the two stages of loading are designed as follows: the first loading could be prestraining the specimens in uniaxial, plane-strain, and biaxial tensions, and the second loading will be covering these three stress states to construct a complete forming limit diagram. These tests usually only involve the change of stress states, but do not involve the change of loading directions, i.e., the major strain direction is mostly along the rolling direction for both first and second-stage loading. As the focus of these tests is the formability of materials under a non-linear strain path, these results are strain-sensitive only.

On the contrary, the stress-sensitive studies on non-monotonic strain paths predominantly focus on the uniaxial tension stress state, especially for the first-step loading, and variation of the loading directions. The two loading stages are commonly designed as one uniaxial tension followed mostly by another uniaxial tension with a different loading direction [7–15] or in some cases by simple shear along different directions [16–18] or biaxial tension [9]. For all these studies, the strategy is to perform the first-step loading on a large uniaxial tensile specimen and then cut small-sized specimens along different loading directions from the initial loading direction to perform the second-step tensile tests. Within this investigation program, the main variables are two: i) the level of prestrain in the first-step loading and ii) the change of the loading directions in the second step. The most investigated change of loading direction is 90° in the physical loading space, and therefore, it is also referred to as cross loading or orthogonal loading. Although certain conclusions on the ductility/formability side could be drawn [19], the focused properties are mainly the stress behavior.

In a nutshell, the following phenomena (also applied to reverse loading) could be identified: i) lower yield strength at reloading than that before unloading, which is also referred to as the Bauschinger effect [20, 21] for reverse loading, ii) higher initial hardening rate at the beginning of reloading, iii) higher yield strength at reloading overshooting the value before unloading, iv) stress stagnation at the initial stage of reloading, v) permanent softening at large strains of reloading. In most cases the phenomena i) lower yield strength is followed by ii) higher initial hardening rate, while iii) higher stress and iv) stress stagnation also appear together. Because these terms are all referend to either yielding or initial straining, they are all defined as *transient behavior*. When the reloading reaches higher strains, no matter the combination of i) and ii) or iii) and iv), the stresses mostly either collapse to the values under monotonic loading or exhibit permanent softening with different stresses but a very similar hardening rate to the monotonic stress–strain curve.

The rather complicated transient behavior has driven many studies in two folds: i) rooting the mechanism in the microstructure level, and ii) developing constitutive models to describe or predict the behavior. Under strain path changes, a most recognized phenomenon on the microstructure level is the evolution of dislocation structures [16, 22–26]. The size and morphology of the dislocations cells upon strain path change could be changed, disrupted, or rearranged. More specifically, for cross loading, additional micro bands could also form inside the dislocation cells [27, 28]. In addition to these morphological-related contributions, studies also show transient behavior is still present even when the dislocations tend to form more homogeneously in grains than forming cells and therefore conclude that the dislocation density might be the key [29]. Whether the dislocations are distributed more homogeneously or in a clustered way, they would introduce long-range back stress, which could impact the plastic deformation after unloading and during reloading [30, 31].

Different from the rather qualitative mechanism mining, the formulation of constitutive models gained many quantitative successes. In general, two types of models have been pursued: the phenomenological models and mechanism-inspired models. The phenomenological models dealing with non-monotonic strain paths could be dated back to the initial kinematic hardening models [32, 33]. During the past decades, many more advanced models have been developed to account for all the phenomena listed above [34–38]. These models have the advantages of reaching high accuracy to describe the plasticity evolution but also suffer from the drawback that many material parameters need to be introduced and calibrated via testing results under non-monotonic strain paths due to their phenomenological nature [39]. On the other hand, mechanism-based models have also been developed utilizing the deep-down physical metallurgy rules and the observation of the dislocation evolution [17, 31]. They became very attractive when these equations are implemented into the crystal plasticity framework as anisotropic features could be also incorporated [39–43]. These models could not compete with the phenomenological models in terms of predictive accuracy [43], but as they are more mechanism-based, they rely on more microstructure observation and need fewer parameters to fit. It shall be also pointed out that the division of these two types of models is not absolute. The phenomenological models, especially the advanced ones, are also very much mechanism-inspired, while the currently developed mechanism-based models are also not completely phenomenological character free, as they also still need a number of experiments to fit their material parameters.

Despite the successes in the mechanism identification and modeling in macro and micro scales, it is evident that the loading mode covered, especially in the first step, is still rather limited to uniaxial tension loading. Studies involving other stress states in the first-step loading indeed exist, e.g., Sang and Lloyd [44] studied the non-monotonic loading of biaxial prestraining followed by uniaxial tension; Wagoner and Laukonis [45] investigated the tensile behavior after plane-strain tension; van Riel and van den Boogaard [46] conducted plane-strain tensile loading followed by orthogonal simple shear; recently Hama et al. [47] performed various strain-path changes after biaxial prestraining using cruciform specimens. However, in general, the deformation mode of the prestraining is much less explored. More importantly, most experimental programs tend to only consider one stress state in prestraining, and the influence of multiple stress states on the non-monotonic stress behavior is not systematically performed and compared.

This study, therefore, aims to conduct a systematic investigation on the stress–strain behavior of non-monotonic strain paths by considering prestraining in three stress states followed by a rotation of the loading axis in the second-stage loading. Inspired by the strain-sensitive studies on non-linear strain paths in the forming limit community, the three stress states include uniaxial, plane-strain, and biaxial tension, which demonstrate very different and non-linear effects on the forming limits for the follow-up deformation. In the current study, we intend to focus on the influence of these prestraining modes on the stress and hardening behavior of an aluminum-magnesium (AlMg) alloy in the follow-up uniaxial tension with and without rotating the loading axis. In addition to the well-known transient behavior, a particular focus will be laid on the strain hardening behavior at large strains. This would create a general condition that is more complex than the state of the art and yet more similar to manufacturing practices in reality. The data generated could be used to further develop, calibrate, and validate both the phenomenological models and/or mechanism-based models. Future analysis of the microstructure changes in this direction would also promote a more concrete understanding of the plastic deformation mechanism at a microstructure and dislocation level.

Materials

The material used in this study is a cold-rolled AA5754 H111 aluminum alloy sheet of 1.5 mm thickness (Provider: Magnealtok). This alloy is in the wrought AlMg family (5xxx series). Its applications include shipbuilding, vehicle bodies, rivets, fishing industry equipment, food processing, etc. H111 stands for the tempering type, and it recognizes that the alloy underwent some amount of cold strain hardening after annealing but not enough for it to qualify as an H11 or H12 tempering [48]. Hereafter, the material is simply referred to as AA5754.

To quantitatively characterize the microstructure features of the material, especially texture, electron backscattered diffraction (EBSD) has been used. Following the strategy by Liu et al. [49] using the cross-sections of both RD-TD (rolling direction–transverse direction) and RD-ND (rolling direction-normal direction) planes to characterize the 3D microstructure features, samples have been obtained from multiple positions from these two planes as shown in Fig. 1c. In the case of RD-TD plane samples, indicated as position 1 in Fig. 1c, ten random measurements spots were taken with an approximate size of 600 μm × 400 μm each, while for the RD-ND plane, given possible microstructure inhomogeneity along the thickness direction, two specific positions, surface corresponding to position 2 and mid-thickness corresponding to position 3 were focused. For each position, five measurements with a similar size to the RD-TD plane were taken to make sure a similar number of grains was collected for the analysis on both planes.

Samples were prepared first by mechanical grinding followed by silica suspension polishing. The step size of the measurement, which corresponds to the edge length of a square pixel, was set as 1 μm. Two typical EBSD measurements are shown in Fig. 1a and b, corresponding to the RD-TD and RD-ND planes, respectively. Grain reconstruction and analysis were carried out by MATLAB/MTEX [50]. The misorientation threshold for the grain reconstruction was 15º. Using all the measurements the total amount of useful grains obtained (excluding edge grains) is 25,141 in the RD-TD plane and 17,521 in the RD-ND plane.

To distinguish if there are texture distinctions between in-plane and through-thickness directions, the {001},

Fig. 1 EBSD orientation maps of AA5754 on (**a**) RD-TD and (**b**) RD-ND planes and (**c**) the illustration of these investigated positions with respect to the sheet metal
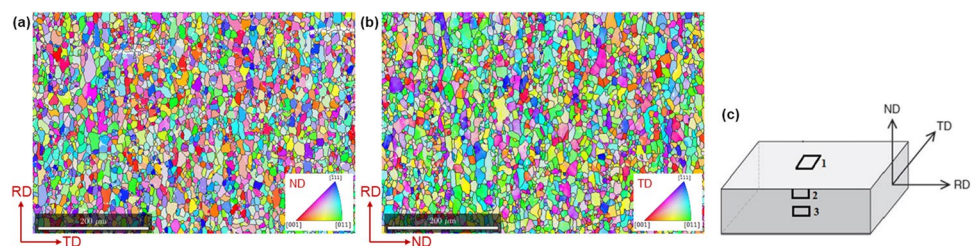
{110}, {111} pole figures analyzed for both RD-TD and RD-ND planes are shown in Fig. 2a. It is seen that the pole figures for these two planes are very similar. Therefore, all the 20 measurements from both planes are assembled for the orientation distribution function (ODF) calculation, as shown in Fig. 2b. Typically rolled face-centered cubic (fcc) metals show the following classic components, copper (Cu), S, and brass (Bs). For the investigated aluminum alloy AA5754, a dominant Cu component is visible, revealed most clearly from the peak points in the {111} pole figure as well as the ODF figure at the section $\varphi_2 = 45°$. In addition, a less dominant S component is also present and a weak Bs component also exists examining the peak points from the ODF figure at the section $\varphi_2 = 0°$. However, it is also noted that the texture intensity of the material is overall rather weak. The texture index defined as the integration of orientation density of an ODF $f(g)$ [50], is also rather small about 1.25.

Experimental setup and program

The experimental program in this study mainly comprises two parts, monotonic tensile loading and non-monotonic tensile loading with two-step straining. For the monotonic tensile tests, classic uniaxial tensile tests with specimens according to ASTM A8 standard were employed. To test the plastic anisotropy behavior of the material, tests were performed along seven different directions, starting from RD with 15° incremental rotations till TD. An Instron 3369 universal tensile test machine was used, combined with the GOM Aramis digital image correlation (DIC)

system for the measurement of global and local strains. The tests were displacement driven and the average strain rate was set as $1 \times 10^{-4} \text{ s}^{-1}$. To ensure the repeatability and statistical information of the material, three parallel tests were performed for each loading direction.

For the non-monotonic strain loading, instead of focusing on only the strain path changes under the stress state of uniaxial tension, the study targets to focus on the combination of stress state change (from different stress states to uniaxial tension) and the change of loading direction (from RD to other directions). The experimental program achieving this is designed and illustrated in Fig. 3. In the first-step loading, three stress states, uniaxial, plane-strain, and biaxial tensions were created by using a hydraulic press and a Marciniak punch with a diameter of 100 mm. After a specific amount of the prestraining without localization or failure, the uniformly deformed area of the Marciniak sample was used to cut mini tensile specimens with dimensions indicated in Fig. 3. The geometry of the specimen followed the ASTM A8 standard but was scaled down with a gauge length of 15 mm to ensure multiple samples along both RD and TD could be cut from the uniformly deformed part of the Marciniak samples.

To decide the level of prestraining to be applied to the first-step loading, trial tests were conducted until any localization and/or early edge fracture was visible. The final amount of prestraining was controlled right below any of these failures for all the stress states. The force of the test was not recorded; however, the strain of the top surface of the Marciniak sample was measured by the GOM Aramis DIC system. Three parallel tests were conducted to ensure good repeatability. For the second-stage loading, the same
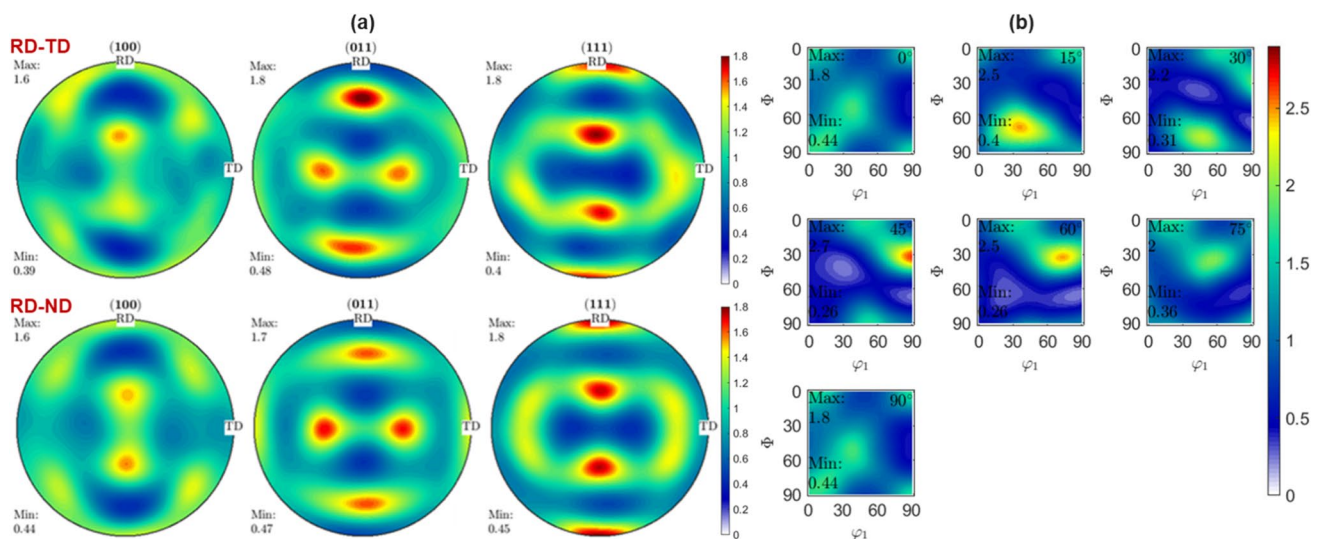

Fig. 2 Texture measurement of AA5754: (**a**) {001}, {110}, {111} pole figures from EBSD on both RD-TD and RD-ND planes; (**b**) ODF figure at different φ_2 sections from EBSD

Fig. 3 Illustration of the experimental procedure of the non-monotonic strain path. Step I: three stress states (uniaxial, plane-strain, and biaxial tensions) along the rolling direction are generated for large Marciniak specimens by a press. Step II, mini tensile test specimens are cut from the large samples along both rolling and transverse directions and then loaded under uniaxial tension (all units in mm)
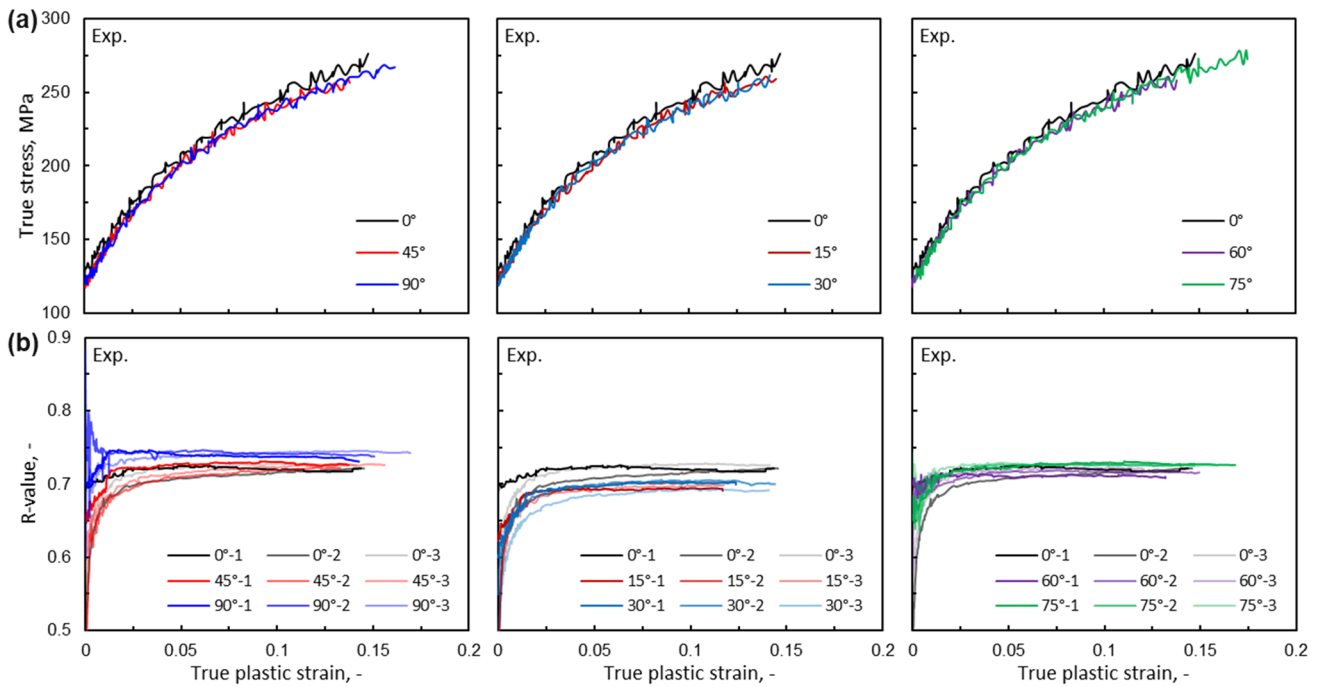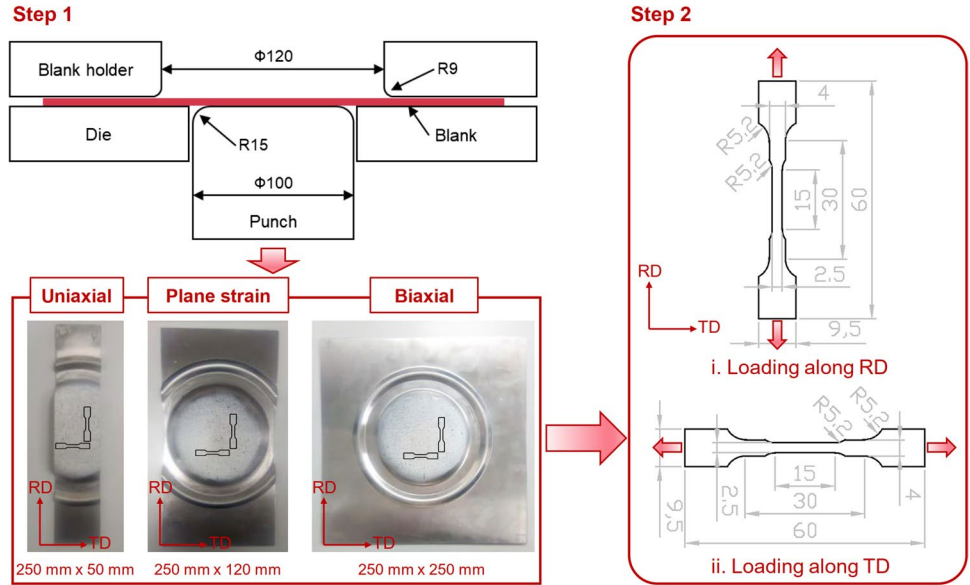

Fig. 4 Mechanical properties of the monotonic uniaxial tensile tests: (**a**) the true stress vs. true plastic strain curves for seven loading directions; (**b**) the r-value evolution curves for seven loading directions

setup of tensile tests as the monotonic ones was used for tests along both RD and TD under a strain rate of 1×10^{-4} s^{-1}.

Results

Monotonic loading

The true stress vs. true plastic strain curves for the monotonic tensile tests along different directions are presented in Fig. 4a. The tensile behavior features serrated stress–strain curves, referred to as the Portevin–Le Chatelier (PLC) effect, which is a typical character of dynamic strain aging (DSA). DSA is observed during plastic deformation of many metallic materials, such as steels [51–56], aluminum alloys [57–59], and titanium alloys [60], at certain ranges of strain rates and temperatures. Different from steels that typically exhibit DSA or PLC at elevated temperatures under quasi-static conditions [51, 52], the aluminum alloy AA5474 shows an obvious effect at room temperature. The origin of the DSA effect lies in dynamic interactions between mobile solid solution (Mg) atoms and dislocations [61]. However, it is not the main focus of the current study to investigate further the DSA side of AA5754.

Although DSA brings certain uncertainty to the evaluation of the stress anisotropy, from Fig. 4a comparing different loading angles with RD, it could be concluded that the material shows a minor stress anisotropy and among the seven loading directions, RD produced the highest stress during the entire plastic deformation. The stresses along TD and diagonal direction (DD) are at a similar level and both about 5% lower than RD at the ultimate tensile strength level. Similar stress levels are also found for loading along 15° and 30° with respect to RD. The stresses loaded along 60° and 75° show somewhat higher values, especially for 75°.

As the second important measure of plastic deformation behavior, the Lankford coefficient (r-values) vs. true plastic strain along seven loading directions are plotted in Fig. 4b. As the results for r-values show a certain level of uncertainty, the three parallel tests are all included. The first feature of all the tests is that the r-values for all seven directions do not show a large difference and vibrate around 0.7. Despite the uncertainty in each direction, the TD loading possesses the highest r-value and it shows a slightly decreasing trend with the plastic deformation. The r-values along RD and DD are showing quite similar values especially when the plastic strain is large and they both show a certain level of an increasing trend, especially for DD, as its value is initially lower than the RD loading at the initial plastic deformation but gets somewhat higher than RD at large strains. The r-values for 15° and 30° loadings are very similar and lower than the RD loading. Starting from DD (45°), an increasing

trend of the r-values with respect to the loading angels is present, and both 60° and 75° loadings reach a similar level of RD, while the values of 75° loading are slightly higher than RD. Different from the loading with rather lower angles (0°-45°), where an increasing trend of the r-value with plastic deformation is found, a decreasing trend of the r-value is dominant for the higher loading angels (60°-90°). Despite these detailed observations of the r-values, together with the very minor planner anisotropy shown in the stress values, it is concluded that the material is generally a transversely isotropic material with slight normal anisotropy.

Non-monotonic loading

In the first-step loading, the change of stress states is achieved via the change of the width of Marciniak samples. It is based on the experience in the forming limit tests, but the exact stress states or strain path still needs to be verified. In addition, it is also important to verify that the planarly deformed part of the sample shows a uniform distribution of strain. Therefore, the major and minor strain distribution of the three strain paths at the end of the first-step loading are presented in Fig. 5a and b, respectively. In the plots, the vertical black line corresponds to RD while the orange horizontal one is along TD. For both major and minor strains, it is clear that a very uniform region right on the planner part of the Marciniak sample is formed. This guarantees that the second-step loading could have homogeneous plastic deformation and repeatability. Furthermore, by reading the distribution of major and minor strains on the legend, it could also be concluded that the desired strain paths are also well achieved. The average strain ratios (minor strain/ major strain) for uniaxial, plane-strain, and biaxial tension are about -0.4, 0, and 1. To be able to make a comparison with the monotonic uniaxial tensile tests, the plastic work or the work-conjugated equivalent strain of these stress states is also needed. However, due to the disadvantage of the current experimental setup using the hydraulic press to deform these large Marciniak samples, the force components are not easy and precise to access. Therefore, it is challenging to obtain a trustworthy stress tensor for the first-step loading. Given the transverse isotropy with minor anisotropy of the material, it is relevant to assume that the simple Mises equivalent strain, according to the following equation, could provide a reasonable estimation of the work-conjugated equivalent strain.

$$\bar{\varepsilon} = \frac{\sqrt{2}}{3} \sqrt{\left(\varepsilon_1 - \varepsilon_2\right)^2 + \left(\varepsilon_1 - \varepsilon_3\right)^2 + \left(\varepsilon_2 - \varepsilon_3\right)^2}$$

$$(1)$$

After performing the second-step loading and applying the equivalent strain from the first-step loading, the true
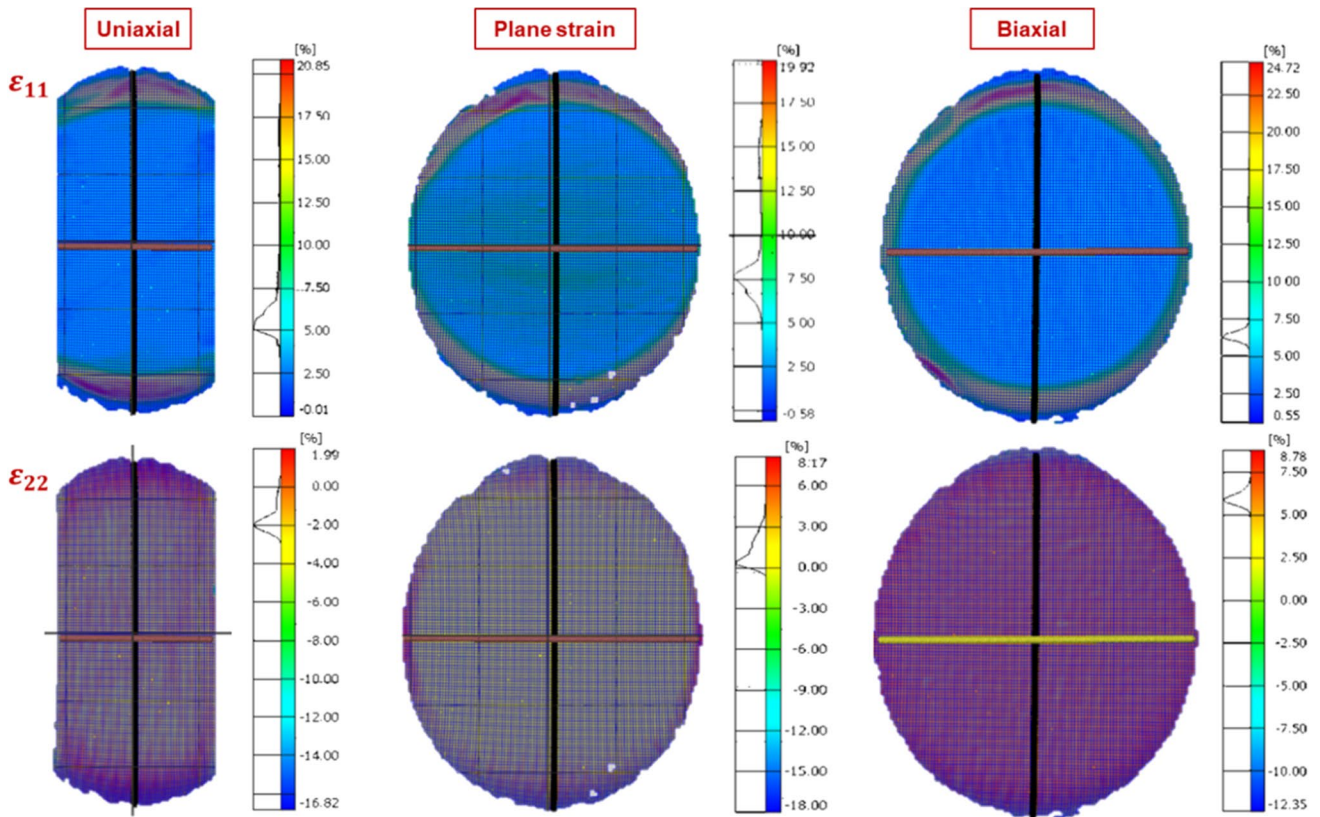
Fig. 5 The distribution of the major strain (ε_{11}) and minor strain (ε_{22}) of the center of Marciniak samples after uniaxial, plane-strain, and biaxial tension pre-loading measured by DIC

Fig. 6 The experimental stress–strain curves of the mini tensile tests along RD and TD in the second-stage loading after pre-straining in comparison with the monotonic stress–strain curves along RD and TD
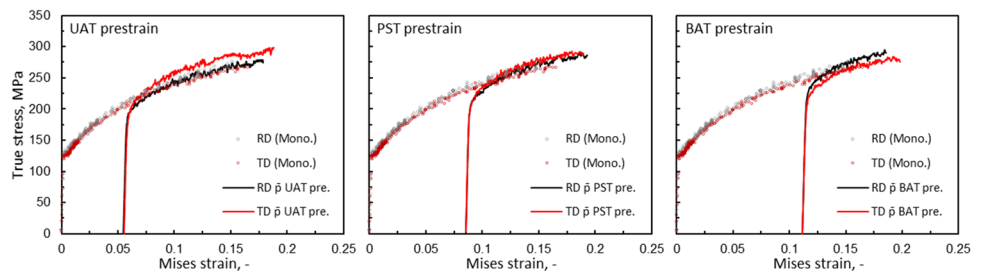
stress–strain curves along both RD and TD from the second-step loading are shifted with the determined Mises prestrain are plotted for the three stress states in Fig. 6. For a better comparison, the stress–strain curves from the monotonic tensile loading along RD and TD are also plotted. Starting from the uniaxial tension (UAT) prestraining, the first observation is that the stress–strain curve of the RD loading after ($\bar{p}$) prestrain is almost identical to the monotonic stress–strain curve along RD, particularly when the strain is large, which confirms that the prestrain path is of high accuracy. However, it is also noted that the yielding of the second-step tensile loading is not reaching the levels of the monotonic loading and a higher strain hardening is present at the beginning of reloading. On the other hand, quite

distinctly, the TD loading after the UAT prestrain presents much higher stresses than the monotonic tests along RD and significantly higher stresses than the monotonic tensile tests along TD. To be more specific, the yielding point is at a similar stress level to the monotonic test along TD, but the hardening rate is substantially larger than in the monotonic case. Very distinctly, this eventually leads to a stress level constantly higher than the monotonic loading along TD.

Moving to the plane-strain tension (PST) mode, the interesting phenomenon is that the stresses in the second-step loading along RD are somewhat higher than the monotonic RD results when the stain gets large, although the initial yielding still shows much lower values. The second-step loading along TD shows similar behavior to the UAT state,

but with a quite lower yield point than the monotonic TD loading. Under the biaxial tension (BAT) loading mode, it is distinct that the second-step loading along RD still shows a lower yield point, but a clear increase of the stresses compared to the monotonic RD at large strains. For the loading along TD, very similar behavior is found to the PST mode, but the amount of stress increase in the non-monotonic strain path compared to the monotonic one is getting weaker.

Discussion

Characterization of the strain path change

The following sections intend to reveal more details concerning the transient and permanent behavior of all the non-monotonic tests and also compare them with each other. To better characterize the level of strain path change, the Schmitt parameter [62, 63] defined below is often used.

$$\alpha = \frac{\dot{\boldsymbol{\varepsilon}}_1^p \, : \, \dot{\boldsymbol{\varepsilon}}_2^p}{\|\dot{\boldsymbol{\varepsilon}}_1^p\|\|\dot{\boldsymbol{\varepsilon}}_2^p\|}$$

(2)

In the equation, $\dot{\boldsymbol{\varepsilon}}_1^p$ and $\dot{\boldsymbol{\varepsilon}}_2^p$ represent the plastic strain rate tensor in the first-step and second-step loading, respectively. Therefore, monotonic loading is corresponding to 1, and reverse loading, e.g., uniaxial tension followed by uniaxial compression is -1. The Schmitt parameter 0 is referred to as cross or orthogonal strain path change. It is noted that this definition is related to the rotation of the strain rate tensor. It shall not be confused with the rotation of the physical loading axes. For example, assuming isotropic materials, rotating the uniaxial tensile loading axes with 90° will result in the Schmitt parameter of -0.5. For convenience, the rotation of the physical loading axes with 90° is referred to as cross loading in this study. Due to either initial anisotropy of materials or some intermediate rotation of loading axes, Schmitt parameters in between these typical values are produced.

For the values in the vicinity of reverse, cross, and monotonic strain path change, they are also referred to as pseudo-reverse, pseudo-cross, and pseudo-monotonic cases [16].

The Schmitt parameter of the six investigated non-monotonic loading cases is estimated and plotted in Fig. 7. As the anisotropy of the material is rather weak, they do not deviate significantly from the ideal values based on isotropy. It is seen that reloading along RD after UAT prestraining is basically a monotonic loading, while along TD it creates a condition in between reverse and cross strain path change. The PST prestraining followed by uniaxial tension is corresponding to more cross strain path change. The reloading along TD gives a Schmitt parameter almost exactly zero, while RD reloading goes towards the positive direction. The BAT prestraining followed by uniaxial tension in both directions gives a Schmitt parameter close to 0.5. It is noted that despite either no change of loading direction (RD to RD) or only change with 90° (RD to TD), the entire program covers quite a large range of the Schmitt parameter from positive to negative, except for -1 for reverse loading.

Transient and permanent behavior after strain path change

To visualize better the influence of the different prestraining modes, they are plotted together with the monotonic cases for RD and TD loading in Fig. 8a and b, respectively. For the RD reloading cases with Schmitt parameter between 0 and 1, although there is no change in the loading angle, only a change of stress state, a clear transient behavior with a lower yield point and very high initial hardening rate is present. When the strain gets larger, a slight to moderate increase of the stresses than the monotonic RD loading (from PST to BAT) is visible. For the cross-loading conditions along TD with the most negative Schmitt parameter, the UAT prestrain gives rise to the most stress increase at large strains, together with a rather lower yield strength compared to the monotonic TD loading. With the loading mode changing to

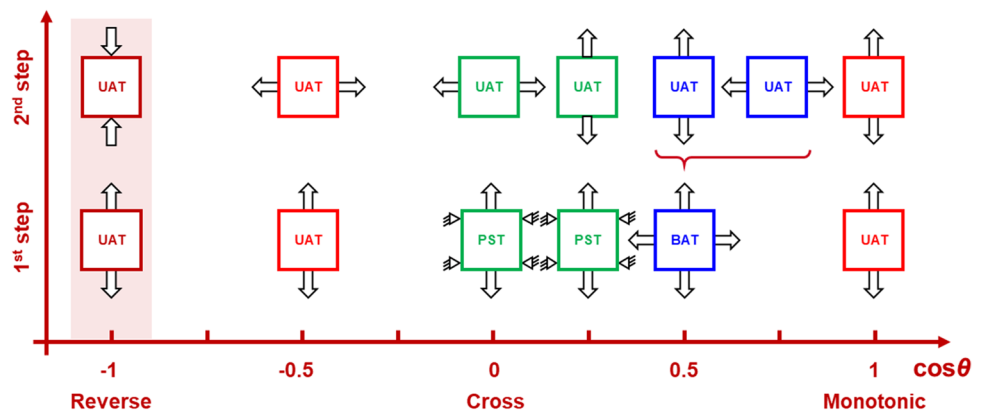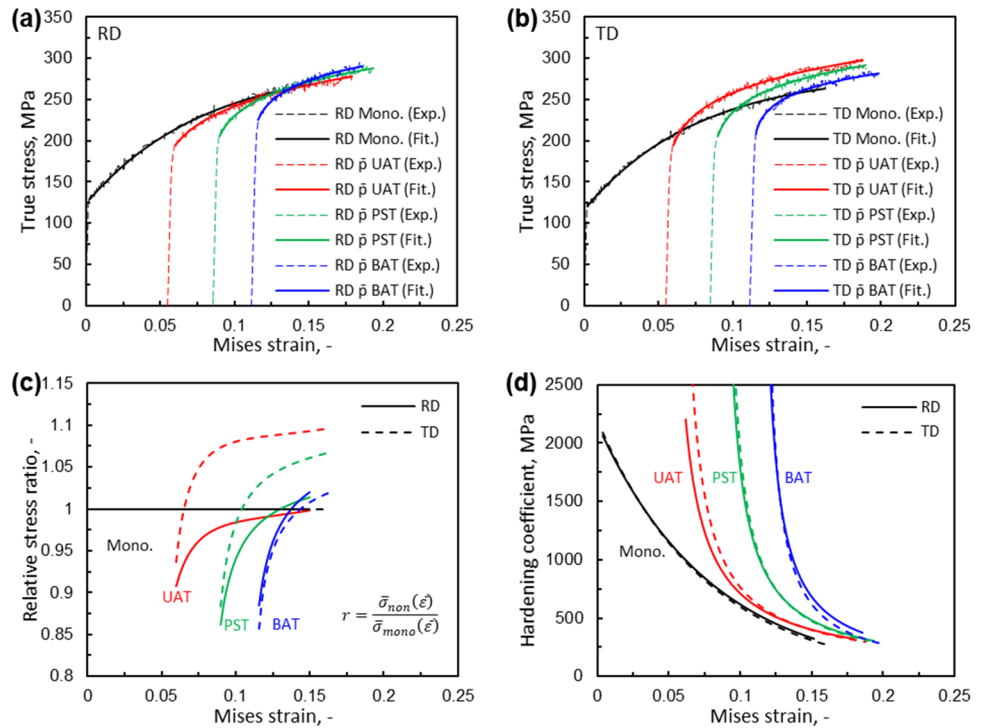**Fig. 7** The Schmitt parameter [62, 63] distribution of the investigated non-monotonic loading cases

Fig. 8 Comparison of the stress–strain curves along RD (**a**) and TD (**b**) for the monotonic and non-monotonic loading cases; (**c**) the relative stress ratio between the non-monotonic and monotonic loading for RD and TD directions; (**d**) the strain hardening rate for all loading cases


PST and BAT (Schmitt parameter from 0 to positive), the additional strain hardening exists but gets decreased and the transient behavior with a decreased yielding is also present.

The serrated flow stresses are also fitted with a Swift-Voce law to smooth curves, with which the relative stress ratios are calculated and plotted in Fig. 8c. The reference stresses for the ratio are the monotonic cases and it is calculated separately for RD and TD loadings throughout the deformation history. Observing Fig. 8c, the developing trend is more clearly demonstrated. For the largest Schmitt parameter condition reloading along RD after UAT, the relative stress ratio is below one up to the uniform strain for monotonic loading along RD. However, the increasing trend is very steady, and as seen in Fig. 8a, the final stress of the non-monotonic loading goes higher with larger strains. For the smallest Schmitt parameter, reloading along TD after UAT, the highest stress ratio is found and about a 10% stress increase is achieved at the end of the uniform strain of

monotonic TD loading. When the Schmitt parameter further increases towards the positive direction, it is concluded that the level of the stress ratios tends to go lower, while a steady increasing trend of the stress ratio during the second-step loading is evident for all cases (above one).

Based on these results across all the covered Schmitt parameters, a unique combination of lower yield points and higher stresses at large strains compared to the monotonic loading prevails. However, for the investigated material, the higher stresses are consistently present at very large strains till the end of uniform deformation, which is different from many previous discoveries in the studies of abrupt strain path changes for either steels or aluminum alloys [7–9, 11–13, 18, 63–68]. To better review its specific features, the typical transient and permanent non-monotonic behavior is summarized in Fig. 9, as indicated by several studies [14, 38, 68]. The reverse loading typically corresponds to a Bauschinger effect with other transient hardening behavior

Fig. 9 Schematic drawing of typical transient and permanent behavior of reverse loading (**a**) and cross loading (**b**), adopted from [14]; the newly discovered feature with a combination of lower yield stress and permanent hardening of non-monotonic loading
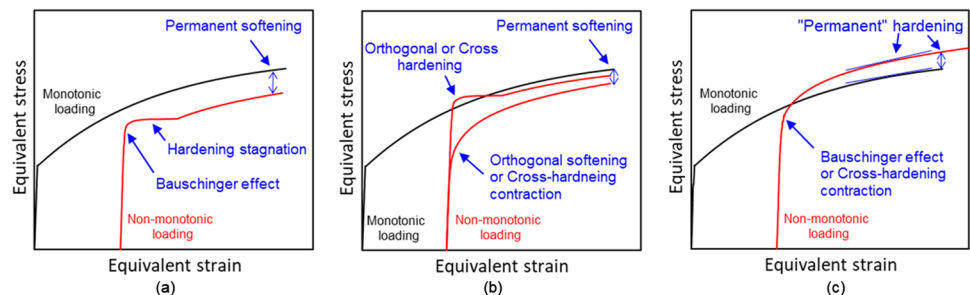
followed by a permanent softening. The cross loading usually shows two types of behavior. The first one is similar to the reverse loading condition with a lower yield stress, which is also referred to as cross-loading contraction [37], leading to eventually permanent softening. The other case is showing much higher yield stress, overshooting the monotonic case, which is also referred to as either cross hardening, latent hardening, or orthogonal hardening. It shall be noted that here the cross hardening is a type of transient behavior as the strain hardening rate is soon becoming smaller or even negative after the stress overshoot and the stress will then in most cases coincide with and eventually follow the monotonic case at large strains or even show permanent softening for some cases [7–9, 11–13, 18, 63–69]. Therefore, the new finding of a steady increase of stresses at large strains till the uniform strain is different from the phenomena observed so far and is referred to as *permanent hardening*.

To further reveal this specific feature, the strain hardening rates for all the monotonic and non-monotonic cases are also calculated and plotted in Fig. 8d. The very high initial hardening rate upon reloading for all non-monotonic cases is evident. More interestingly, the strain hardening rate at large strains is found also consistently above the monotonic case, which eventually contributes to the steady increases in stresses as shown in Fig. 8a-c. Therefore, this adds another meaning to permanent hardening, that it is not just implying the increase of absolute values of the stresses, but also the increase in the strain hardening rate caused by non-monotonic loading. This finding is also in line with the longer uniform strain of the non-monotonic loadings compared to the monotonic case, seen in Fig. 8a, b, and d. The additional strain hardening rate is postponing the deformation instability under non-monotonic loading, which is not common to see in literature as reviewed above and is beneficial for the material forming processes in general.

The discovered "permeant hardening" is new compared to most alloys and metals under tension-tension or rolling-tension loadings [7–9, 11–13, 18, 65–68]. It shall be noted that the permanent hardening, only in the sense of the absolute values of stresses at large strains, has been also observed in tension-shear loading. Barlat et al. [16] conducted non-monotonic tension-shear tests on AA1050-O and found higher stresses at large strains under cross-loading conditions; however, at pseudo-reverse and pseudo-monotonic regimes, lower yield strength and permanent softening behavior were obvious. A very similar experimental program was conducted by Rauch and Schmitt [24] for a low-carbon steel and they discovered the same conclusion. Peeters et al. [41, 42] performed non-monotonic tension-shear and shear-shear loading, and found also higher stresses at large strains under cross loading in the tension-shear mode, while in the shear-shear loading with changes of multiple loadings angles, only transient

cross-hardening behavior followed by coinciding with the monotonic stresses was found. According to texture analysis and crystal plasticity simulation by Lopes et al. [25] and Barlat et al. [16], they concluded that the higher stresses at large strain under cross loading in the tension-shear mode should be mainly caused by texture evolution and therefore, the crystal plasticity model accounting for only texture evolution could predict the higher stresses at large strains. In the current study, since the material is rather isotropic and the loadings are all in tension mode, the texture evolution effect shall be considered minor. Therefore, the cause of permanent hardening seems to be more related to the micro-level deformation mechanism involving dislocation interactions. This hypothesis could be also supported by the unique observation of the higher strain hardening rate at larger strains compared to the monotonic loading, which, according to the best knowledge of the authors, has not been reported in existing alloys or steels even in tension-shear loading mode.

More interestingly, as studied in numerous non-monotonic loading with strain path changes either tension-tension, tension-shear, or tension–compression, it is common and almost without exception that for reverse, pseudo-reverse, and pseudo-monotonic loading, lower yield stress and permanent softening are revealed; however, in the investigated AA5754, the permanent hardening, in terms of both stress and hardening rate, is evident not only for cross loading but for all cases including pseudo-monotonic and pseudo-reverse loading. Although the reloading along TD after UAT prestraining in RD is not exactly pseudo-reverse loading, more in between cross and reverse loading (Fig. 7), it is also surprising to notice that this case is creating the largest amount of permanent hardening as shown in Fig. 8a-c. With the increase of the Schmitt parameter, the level of the permanent hardening seems to be decreased, as seen from the relative stress ratio between the reloading stress vs. the monotonic ones in Fig. 8c. This seems contradictory to the common understanding of cross (latent) hardening, which assumes that its effect is maximized under cross strain path change, i.e., Schmitt parameter as zero, as microscopically it corresponds to deactivating the slip systems from first-step loading and activating news ones [24, 69, 70]. However, as permanent hardening is a different phenomenon from the cross or latent hardening, more systematic studies in monitoring the microstructure evolution and numerical modeling are needed to reveal the mechanisms. One possible hypothesis for this phenomenon is the existence of DSA in this aluminum alloy. Most likely, the specific distribution and interaction of the solute atoms with dislocations in the first-step loading would still promote the strain hardening in the second-stage loading after the reorientation of slip systems at

Fig. 10 Normalized stresses (stress along TD loading over RD) at three strain levels for all monotonic and the second-step loading of the non-monotonic case. The strains for the reloading of the non-monotonic case are calculated without the accumulation of the prestrain in the first-step loading
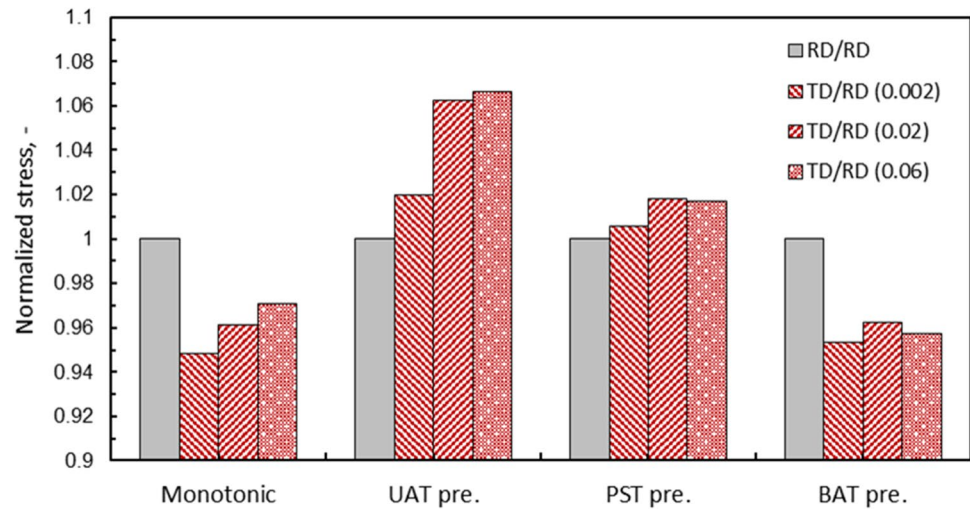
the initial reloading. In addition, other tensile directions, e.g., 45° with respect to RD and reverse loading will be also investigated to further examine the non-monotonic loading behavior of this material.

Evolution of anisotropy after pre-deformation

In addition to characterizing the non-monotonic behavior of materials, which is beneficial to understanding and guiding the material forming processes, to further investigate the evolution of anisotropy after pre-deformation is also meaningful for assessing the material performance after forming. In Fig. 10, the normalized stress (ratio of stresses along TD over RD) is calculated for both the monotonic loading and the reloading after three types of prestraining. For each case, three strain levels are considered to evaluate the stress anisotropy evolution. It is noted that here different from previous sections the strains for the reloading cases are considered without their previous accumulation. It is intended to treat the pre-deformed material as new and compare its anisotropy with the original status. As the actual stresses along RD loading are used as the reference ones, the RD/RD case is always one for three strain levels.

The initial microstructure features minor anisotropy with TD stress about 5% less than RD, and this difference decreases to less than 3%, when strains get larger, as shown in Fig. 10 for the monotonic case. After UAT prestraining, the stress anisotropy shows an opposite pattern, and the TD stress overshoots the RD case by about 8% at large strains. For the PST prestraining, the anisotropic behavior for the second-step loading is getting very minimum, and the stress difference between RD and TD is within 2%. Interestingly, the anisotropic behavior of the material after BAT prestraining is similar to the initial one, RD higher than TD with a difference within 5%. This is also somewhat

in line with the intuition, as the BAT loadings give equal in-plane deformation along RD and TD and do not seem to introduce a directional deformation, whereas the UAT provides the most distinctive deformation anisotropy in terms of strains along RD and TD, and PST falls right in between UAT and BAT. Overall, it is concluded that pre-deformation could make a substantial impact on the material anisotropy and the evolution of the anisotropy could be strongly dependent on the stress state of pre-deformation. Correlating with the reasoning of non-monotonic loading, the cause of the anisotropy evolution is not on the level of texture evolution, but rather micro level involving dislocation interactions with each other or solute atoms on different slip systems.

Conclusions

- A comprehensive experimental program with abrupt strain path changes is designed for an aluminum alloy (AA5754) by combing first-step loading along rolling direction (RD) under three stress states, uniaxial, plane-strain, and biaxial tensions with the second-step uniaxial tensile loading along both RD and transverse direction (TD). These tension-tension strain paths by changing stress states and loading axes create a wide and distributed spectrum of the Schmitt parameter from most positive to negative values.
- For most of the non-monotonic strain paths, a unique phenomenon featuring a lower yield strength at reloading and a steady increase of stress finally overshooting the monotonic case at intermediate or large strains is discovered. Different from the cross or latent hardening as a transient behavior, this hardening behavior is consistent and causes an increase in the strain harden-

ing rate compared to the monotonic case. It is, therefore, referred to as permanent hardening. As the material is rather isotopic and the texture evolution effect is minor during tension-tension strain path changes, it is speculated that the reason for it shall be related to microscopic dislocation interactions with each other at different slip systems and even with the solute atoms, which play a significant role in the plastic deformation for the investigated material showing clear dynamic strain aging behavior.

- For uniaxial reloading along RD after prestraining in different modes along RD, the stress increase compared with the monotonic case by permanent hardening is rather minor, while for the cross loading along TD with Schmitt parameter close to or smaller than zero, the stress increase at large strains of the reloading gets higher. A maximum increase of stress with about 10% is found for the TD reloading after uniaxial tension prestraining in RD compared with the monotonic TD loading, although its Schmitt parameter deviates further from zero than the TD reloading after plane-strain tension. This is different from the cross or latent hardening, which is expected to have a maximum stress increase at the Schmitt parameter of zero.

- Pre-deformation makes a substantial impact on the material anisotropy. The evolution of anisotropy is strongly dependent on the stress state of pre-deformation. For the investigated material, the in-plane biaxial tension makes the minimum impact on the material anisotropy, while the uniaxial tension prestraining imposes substantial evolution of stress anisotropy of the material.

Declarations

Conflicts of interests The authors declare that they have no conflict of interest.

References

1. Chin-Chan C (1982) An investigation of the strain path dependence of the forming limit curve. Int J Solids Struct 18(3):205–215. https://doi.org/10.1016/0020-7683(82)90003-8

2. Barata da Rocha A, Barlat F, Jalinier JM (1985) Prediction of the forming limit diagrams of anisotropic sheets in linear and non-linear loading. Mater Sci Eng 68(2):151–164. https://doi.org/10.1016/0025-5416(85)90404-5

3. Graf A, Hosford W (1994) The influence of strain-path changes on forming limit diagrams of A1 6111 T4. Int J Mech Sci 36(10):897–910. https://doi.org/10.1016/0020-7403(94)90053-1

4. Stoughton TB (2000) A general forming limit criterion for sheet metal forming. Int J Mech Sci 42(1):1–27. https://doi.org/10.1016/S0020-7403(98)00113-1

5. Kuroda M, Tvergaard V (2000) Effect of strain path change on limits to ductility of anisotropic metal sheets. Int J Mech Sci 42(5):867–887. https://doi.org/10.1016/S0020-7403(99)00029-6

6. Manopulo N, Hora P, Peters P, Gorji M, Barlat F (2015) An extended Modified Maximum Force Criterion for the prediction of localized necking under non-proportional loading. Int J Plast 75:189–203

7. Ha J, Lee M-G, Barlat F (2013) Strain hardening response and modeling of EDDQ and DP780 steel sheet under non-linear strain path. Mech Mater 64:11–26. https://doi.org/10.1016/j.mechmat.2013.04.004

8. Wen W, Borodachenkova M, Tomé CN, Vincze G, Rauch EF, Barlat F et al (2015) Mechanical behavior of Mg subjected to strain path changes: Experiments and modeling. Int J Plast 73:171–183. https://doi.org/10.1016/j.ijplas.2014.10.009

9. Zaman SB, Barlat F, Kim J-H (2018) Deformation-induced anisotropy of uniaxially prestrained steel sheets. Int J Solids Struct 134:20–29. https://doi.org/10.1016/j.ijsolstr.2017.10.029

10. Vincze G, Barlat F, Rauch EF, Tomé CN, Butuc MC, Grácio JJ (2013) Experiments and modeling of low carbon steel sheet subjected to double strain path changes. Metall and Mater Trans A 44(10):4475–4479. https://doi.org/10.1007/s11661-013-1895-4

11. Vincze G, Butuc MC, Barlat F, Lopes AB, Silva TFV (2019) Strain path changes in aluminum. AIP Conf Proc 2113(1):160013. https://doi.org/10.1063/1.5112710

12. Tarigopula V, Hopperstad OS, Langseth M, Clausen AH (2008) Elastic-plastic behaviour of dual-phase, high-strength steel under strain-path changes. Eur J Mech A Solids 27(5):764–782. https://doi.org/10.1016/j.euromechsol.2008.01.002

13. Mánik T, Holmedal B, Hopperstad OS (2015) Strain-path change induced transients in flow stress, work hardening and r-values in aluminum. Int J Plast 69:1–20. https://doi.org/10.1016/j.ijplas.2015.01.004

14. Qin J, Holmedal B, Hopperstad OS (2018) A combined isotropic, kinematic and distortional hardening model for aluminum and steels under complex strain-path changes. Int J Plast 101:156–169. https://doi.org/10.1016/j.ijplas.2017.10.013

15. Wilson DV, Zandrahimi M, Roberts WT (1990) Effects of changes in strain path on work-hardening in CP aluminium and an Al-Cu-Mg alloy. Acta Metall Mater 38(2):215–226. https://doi.org/10.1016/0956-7151(90)90051-H

16. Barlat F, Duarte JMF, Gracio JJ, Lopes AB, Rauch EF (2003) Plastic flow for non-monotonic loading conditions of an aluminum alloy sheet sample. Int J Plast 19(8):1215–1244. https://doi.org/10.1016/S0749-6419(02)00020-7

17. Rauch EF, Gracio JJ, Barlat F, Vincze G (2011) Modelling the plastic behaviour of metals under complex loading conditions. Model Simul Mater Sci 19(3):035009. https://doi.org/10.1088/0965-0393/19/3/035009

18. Wen W, Borodachenkova M, Tomé CN, Vincze G, Rauch EF, Barlat F et al (2016) Mechanical behavior of low carbon steel subjected to strain path changes: Experiments and modeling. Acta Mater 111:305–314. https://doi.org/10.1016/j.actamat.2016.03.075

19. Li F, Bate PS (1991) Strain path change effects in cube textured aluminium sheet. Acta Metall Mater 39(11):2639–2650. https://doi.org/10.1016/0956-7151(91)90080-K

20. Bauschinger J (1881) Changes of the elastic limit and the modulus of elasticity on various metals. Zivilingenieur 27:289–348

21. Hasegawa T, Yakou T, Karashima S (1975) Deformation behaviour and dislocation structures upon stress reversal in polycrystalline aluminium. Mater Sci Eng 20:267–276. https://doi.org/10.1016/0025-5416(75)90159-7

22. Rao BVN, Laukonis JV (1983) Microstructural mechanism for the anomalous tensile behavior of aluminum-killed steel prestrained in plane strain tension. Mater Sci Eng 60(2):125–135. https://doi.org/10.1016/0025-5416(83)90182-9

23. Fernandes JV, Schmitt JH (1983) Dislocation microstructures in steel during deep drawing. Philos Mag A 48(6):841–870. https://doi.org/10.1080/01418618308244323

24. Rauch EF, Schmitt JH (1989) Dislocation substructures in mild steel deformed in simple shear. Mater Sci Eng, A 113:441–448. https://doi.org/10.1016/0921-5093(89)90331-6

25. Lopes AB, Barlat F, Gracio JJ, Ferreira Duarte JF, Rauch EF (2003) Effect of texture and microstructure on strain hardening anisotropy for aluminum deformed in uniaxial tension and simple shear. Int J Plast 19(1):1–22. https://doi.org/10.1016/S0749-6419(01)00016-X

26. Clausmeyer T, Gerstein G, Bargmann S, Svendsen B, van den Boogaard AH, Zillmann B (2013) Experimental characterization of microstructure development during loading path changes in bcc sheet steels. J Mater Sci 48(2):674–689. https://doi.org/10.1007/s10853-012-6780-9

27. Thuillier S, Rauch EF (1994) Development of microbands in mild steel during cross loading. Acta Metall Mater 42(6):1973–1983. https://doi.org/10.1016/0956-7151(94)90022-1

28. Rauch EF, Thuillier S (1993) Rheological behaviour of mild steel under monotonic loading conditions and cross-loading. Mater Sci Eng A 164(1):255–259. https://doi.org/10.1016/0921-5093(93)90673-3

29. Rauch EF (1997) The stresses and work hardening rates of mild steel with different dislocation patterns. Mater Sci Eng A 234–236:653–656. https://doi.org/10.1016/S0921-5093(97)00357-2

30. Mughrabi H (1983) Dislocation wall and cell structures and long-range internal stresses in deformed metal crystals. Acta Metall 31(9):1367–1379. https://doi.org/10.1016/0001-6160(83)90007-X

31. Goerdeler M, Gottstein G (2001) A microstructural work hardening model based on three internal state variables. Mater Sci Eng, A 309–310:377–381. https://doi.org/10.1016/S0921-5093(00)01728-7

32. Prager W (1949) Recent developments in the mathematical theory of plasticity. J Appl Phys 20(3):235–241. https://doi.org/10.1063/1.1698348

33. Chaboche JL (1986) Time-independent constitutive theories for cyclic plasticity. Int J Plast 2(2):149–188. https://doi.org/10.1016/0749-6419(86)90010-0

34. Yoshida F, Uemori T (2002) A model of large-strain cyclic plasticity describing the Bauschinger effect and workhardening stagnation. Int J Plast 18(5):661–686. https://doi.org/10.1016/S0749-6419(01)00050-X

35. Lee M-G, Kim D, Kim C, Wenner ML, Wagoner RH, Chung K (2007) A practical two-surface plasticity model and its application to spring-back prediction. Int J Plast 23(7):1189–1212. https://doi.org/10.1016/j.ijplas.2006.10.011

36. Barlat F, Gracio JJ, Lee MG, Rauch EF, Vincze G (2011) An alternative to kinematic hardening in classical plasticity. Int J Plast 27(9):1309–1327. https://doi.org/10.1016/j.ijplas.2011.03.003

37. Barlat F, Vincze G, Gracio JJ, Lee MG, Rauch EF, Tome CN (2014) Enhancements of homogenous anisotropic hardening model and application to mild and dual-phase steels. Int J Plast 58:201–218

38. Barlat F, Yoon S-Y, Lee S-Y, Wi M-S, Kim J-H (2020) Distortional plasticity framework with application to advanced high strength steel. Int J Solids Struct 202:947–962. https://doi.org/10.1016/j.ijsolstr.2020.05.014

39. Jeong Y, Barlat F, Tomé CN, Wen W (2017) A comparative study between micro- and macro-mechanical constitutive models developed for complex loading scenarios. Int J Plast 93:212–228. https://doi.org/10.1016/j.ijplas.2016.07.015

40. Kitayama K, Tomé CN, Rauch EF, Gracio JJ, Barlat F (2013) A crystallographic dislocation model for describing hardening of polycrystals during strain path changes. Application to low carbon steels. Int J Plast 46:54–69. https://doi.org/10.1016/j.ijplas.2012.09.004

41. Peeters B, Kalidindi SR, Van Houtte P, Aernoudt E (2000) A crystal plasticity based work-hardening/softening model for b.c.c. metals under changing strain paths. Acta Mater 48(9):2123–33. https://doi.org/10.1016/S1359-6454(00)00047-1

42. Peeters B, Seefeldt M, Teodosiu C, Kalidindi SR, Van Houtte P, Aernoudt E (2001) Work-hardening/softening behaviour of b.c.c. polycrystals during changing strain paths: I. An integrated model based on substructure and texture evolution, and its prediction of the stress–strain behaviour of an IF steel during two-stage strain paths. Acta Mater 49(9):1607–19. https://doi.org/10.1016/S1359-6454(01)00066-0

43. Kim H, Barlat F, Lee Y, Zaman SB, Lee CS, Jeong Y (2018) A crystal plasticity model for describing the anisotropic hardening behavior of steel sheets during strain-path changes. Int J Plast 111:85–106. https://doi.org/10.1016/j.ijplas.2018.07.010

44. Sang H, Lloyd DJ (1979) The influence of biaxial prestrain on the tensile properties of three aluminum alloys. Metall Trans A 10(11):1773–1776. https://doi.org/10.1007/BF02811714

45. Wagoner RH, Laukonis JV (1983) Plastic behavior of aluminum-killed steel following plane-strain deformation. Metall Trans A 14(7):1487–1495. https://doi.org/10.1007/BF02664833

46. van Riel M, van den Boogaard AH (2007) Stress–strain responses for continuous orthogonal strain path changes with increasing sharpness. Scripta Mater 57(5):381–384. https://doi.org/10.1016/j.scriptamat.2007.05.005

47. Hama T, Namakawa R, Maeda Y, Maeda Y (2021) Prediction of work-hardening behavior under various loading paths in 5083-O aluminum alloy sheet using crystal plasticity models. Mater Trans 62(8):1124–1132. https://doi.org/10.2320/matertrans.MT-M2021020

48. Kaufman JG (2000) Introduction to aluminum alloys and tempers. ASM international, Materials Park

49. Liu W, Lian J, Aravas N, Münstermann S (2020) A strategy for synthetic microstructure generation and crystal plasticity parameter calibration of fine-grain-structured dual-phase steel. Int J Plast 126:102614. https://doi.org/10.1016/j.ijplas.2019.10.002

50. Bachmann F, Hielscher R, Schaeben H (2010) Texture Analysis with MTEX – Free and Open Source Software Toolbox. Solid State Phenom 160:63–68. https://doi.org/10.4028/www.scientific.net/SSP.160.63

51. Liu W, Lian J (2021) Stress-state dependence of dynamic strain aging: Thermal hardening and blue brittleness. Int J Miner Metall Mater 28(5):854–866. https://doi.org/10.1007/s12613-021-2250-1

52. Shen F, Münstermann S, Lian J (2020) An evolving plasticity model considering anisotropy, thermal softening and dynamic

strain aging. Int J Plast 132:102747. https://doi.org/10.1016/j.ijplas.2020.102747

53. Lee S-J, Kim J, Kane SN, Cooman BCD (2011) On the origin of dynamic strain aging in twinning-induced plasticity steels. Acta Mater 59(17):6809–6819. https://doi.org/10.1016/j.actamat.2011.07.040

54. Wang XG, Wang L, Huang MX (2017) Kinematic and thermal characteristics of Lüders and Portevin-Le Châtelier bands in a medium Mn transformation-induced plasticity steel. Acta Mater 124:17–29. https://doi.org/10.1016/j.actamat.2016.10.069

55. Yang F, Luo H, Pu E, Zhang S, Dong H (2018) On the characteristics of Portevin–Le Chatelier bands in cold-rolled 7Mn steel showing transformation-induced plasticity. Int J Plast 103:188–202. https://doi.org/10.1016/j.ijplas.2018.01.010

56. Chandran S, Liu W, Lian J, Münstermann S, Verleysen P (2022) Dynamic strain aging in DP1000: Effect of temperature and strain rate. Mater Sci Eng A 832:142509. https://doi.org/10.1016/j.msea.2021.142509

57. Aboulfadl H, Deges J, Choi P, Raabe D (2015) Dynamic strain aging studied at the atomic scale. Acta Mater 86:34–42. https://doi.org/10.1016/j.actamat.2014.12.028

58. Benallal A, Berstad T, Børvik T, Hopperstad OS, Koutiri I, de Codes RN (2008) An experimental and numerical investigation of the behaviour of AA5083 aluminium alloy in presence of the Portevin–Le Chatelier effect. Int J Plast 24(10):1916–1945. https://doi.org/10.1016/j.ijplas.2008.03.008

59. Kreyca J, Kozeschnik E (2018) State parameter-based constitutive modelling of stress strain curves in Al-Mg solid solutions. Int J Plast 103:67–80. https://doi.org/10.1016/j.ijplas.2018.01.001

60. Cheng J, Nemat-Nasser S (2000) A model for experimentally-observed high-strain-rate dynamic strain aging in titanium. Acta Mater 48(12):3131–3144. https://doi.org/10.1016/S1359-6454(00)00124-5

61. Neuhäuser H, Klose FB, Hagemann F, Weidenmüller J, Dierke H, Hähner P (2004) On the PLC effect in strain-rate and stress-rate controlled tests–studies by laser scanning extensometry. J Alloy Compd 378(1):13–18. https://doi.org/10.1016/j.jallcom.2003.10.064

62. Schmitt JH, Aernoudt E, Baudelet B (1985) Yield loci for polycrystalline metals without texture. Mater Sci Eng 75(1):13–20. https://doi.org/10.1016/0025-5416(85)90173-9

63. Schmitt JH, Shen EL, Raphanel JL (1994) A parameter for measuring the magnitude of a change of strain path: Validation and comparison with experiments on low carbon steel. Int J Plast 10(5):535–551. https://doi.org/10.1016/0749-6419(94)90013-2

64. Holmedal B, Houtte PV, An Y (2008) A crystal plasticity model for strain-path changes in metals. Int J Plast 24(8):1360–1379. https://doi.org/10.1016/j.ijplas.2007.09.007

65. Qin J, Holmedal B, Zhang K, Hopperstad OS (2017) Modeling strain-path changes in aluminum and steel. Int J Solids Struct 117:123–136. https://doi.org/10.1016/j.ijsolstr.2017.03.032

66. Qin J, Holmedal B, Hopperstad OS (2019) Experimental characterization and modeling of aluminum alloy AA3103 for complex single and double strain-path changes. Int J Plast 112:158–171. https://doi.org/10.1016/j.ijplas.2018.08.011

67. Kim D, Barlat F, Bouvier S, Rabahallah M, Balan T, Chung K (2007) Non-quadratic anisotropic potentials based on linear transformation of plastic strain rate. Int J Plast 23(8):1380–1399

68. Lee S-Y, Kim J-M, Kim J-H, Barlat F (2020) Validation of homogeneous anisotropic hardening model using non-linear strain path experiments. Int J Mech Sci 183:105769. https://doi.org/10.1016/j.ijmecsci.2020.105769

69. Gutknecht F, Traphöner H, Clausmeyer T, Tekkaya AE (2021) Characterization of flow induced anisotropy in sheet metal at large strain. Exp Mech. https://doi.org/10.1007/s11340-021-00776-9

70. Barlat F, Richmond O (2003) Modelling macroscopic imperfections for the prediction of flow localization and fracture. Fatigue Fract Eng Mater Struct 26(4):311–321. https://doi.org/10.1046/j.1460-2695.2003.00470.x